Estimating Enhanced Fujita Scale Levels Based on Forest Damage Severity

CHRISTOPHER M. GODFREY

Department of Atmospheric Sciences, University of North Carolina at Asheville, Asheville, North Carolina

CHRIS J. PETERSON

Department of Plant Biology, The University of Georgia, Athens, Georgia

(Manuscript received 23 May 2016, in final form 30 September 2016)

ABSTRACT

Enhanced Fujita (EF) scale estimates following tornadoes remain challenging in rural areas with few traditional damage indicators. In some cases, such as the 27 April 2011 tornadoes that passed through mostly inaccessible terrain in the Great Smoky Mountains National Park and the Chattahoochee National Forest in the southeastern United States, traditional ground-based tornado damage surveys are nearly impossible. This work presents a novel method to infer EF-scale categories in forests using levels of tree damage and a coupled wind and tree resistance model. High-resolution aerial imagery allows detailed analyses based on a field of nearly half a million trees labeled with their geographic location and fall direction. Ground surveys also provide details on the composition of tree species and tree diameters within each tornado track. A statistical resampling procedure randomly draws a sample of trees from this database of observed trees. The coupled wind and tree resistance model determines the percentage of trees in that sample that fall for a given wind speed. By repeating this procedure, each wind speed value corresponds with a distribution of treefall percentages in the sampled plots. Comparing these results with the observed treefall percentage in small subplots along the entire tornado track allows estimation of the most probable wind speed associated with each subplot. Maps of estimated EF-scale levels reveal the relationship between complex terrain and wind speeds and show the variability of the intensity of each tornado along both tracks. This approach may lead to methods for the straightforward estimation of EF-scale categories in remote or inaccessible locations.

1. Introduction

A reliable tornado climatology relies on accurate estimates of tornado pathlength, width, and intensity. Edwards et al. (2013) point out the difficulty of such estimates, even after the adoption of the enhanced Fujita (EF) scale (WSEC 2006), which relies on the availability of a selection of damage indicators (DIs) within the damage swath of a tornado. It remains particularly challenging to assign wind speed estimates in rural areas with few traditional DIs, as in dense forests. Yet forests account for over 60% of the total land area of the southeastern United States (Oswalt et al. 2014), making typical ground-based damage assessments rather difficult in these areas.

For example, several 27 April 2011 long-track tornadoes passed through heavily forested and often inaccessible terrain across the southern Appalachian Mountains. One tornado, rated EF4, traveled 18 mi over the western portion of the Great Smoky Mountains National Park (GSMNP) in eastern Tennessee. This tornado received its rating based on a single damage indicator—the tornado collapsed a metal truss tower along an electrical transmission line (NWS Morristown, Tennessee, 2011, personal communication). Although the upper bound for this particular damage indicator is near the peak of the range of wind speeds corresponding with an EF3 rating, the surveyor noted the extraordinary damage to the trees in the area and decided to augment the rating to an EF4. A second tornado, rated EF3,

Denotes Open Access content.

Corresponding author e-mail: Dr. Christopher M. Godfrey, cgodfrey@unca.edu

DOI: 10.1175/WAF-D-16-0104.1

traveled 38 mi across the mountains of northern Georgia in the Chattahoochee National Forest (CNF). This tornado received its rating based on damage to numerous structures near the very end of its long path. In both cases, the vast majority of the tornado track remained inaccessible to surveyors on the ground because of the absence of roads or trails. These rare and notable events provide a unique and valuable opportunity to assess tornadic winds in heavily forested and mountainous areas through analyses of forest damage.

Research on observed tornado behavior in rough terrain remains limited in the peer-reviewed literature. Fujita (1989) performs a detailed analysis of the forest damage patterns produced by a violent tornado in the mountainous terrain of northwest Wyoming. Dunn and Vasiloff (2001) examine the Doppler radar presentation of a tornado that passed through Salt Lake City, Utah, and note the similarity between the damage patterns in a forested area outside the city with those observed by Fujita (1989). Following an analysis of damage patterns produced by several Pennsylvania tornadoes, Forbes (1998) lists some common characteristics of damage patterns in relation to certain topographic features. Cannon et al. (2016) use vertical aerial photographs to characterize tornado damage severity along the same two tornado tracks discussed in the present study and provide evidence that suggests that damage severity decreases as tornadoes ascend ridges and increases as they descend into valleys. Bluestein (2000) analyzes a tornado in the high terrain of Colorado, while LaPenta et al. (2005) and Bosart et al. (2006) review case studies of tornadoes in complex terrain in eastern New York and western Massachusetts, respectively. Numerous authors use numerical simulations to study near-surface tornado dynamics (e.g., Dessens 1972; Fiedler 1994; Fiedler and Rotunno 1986; Lewellen and Lewellen 2007; Lewellen et al. 1997; Lewellen et al. 2000, 2008; Roberts et al. 2016; Schenkman et al. 2014), but only recently has anyone attempted to incorporate very simple terrain variations into either supercell simulations (e.g., Homar et al. 2003; Markowski and Dotzek 2011; Smith et al. 2016) or models that explicitly resolve tornado-like vortices (Lewellen 2012). Thus, observational studies that characterize the near-surface tornadic wind field in complex topography remain vitally important.

Previous studies of tornado tracks through forests (e.g., Bech et al. 2009; Beck and Dotzek 2010; Blanchard 2013) suggest that the orientation and degree of damage of fallen trees will allow a reconstruction of the near-surface wind field. Letzmann (1925) presents the original foundation for this type of analysis and derives predictions of surface-level wind fields based on analytical solutions to simple Rankine vortex events. By assuming that trees fall in the direction of the wind at the moment the force exceeds their rooting or trunk strength, Letzmann (1925) notes that the spatial patterns of fallen trees, and their orientations, preserve a signature of the surface-level winds as a tornado moves over a forested landscape. More recently, Holland et al. (2006) combine Letzmann's (1925) wind field model with forestry models of tree stability developed by Peltola and Kellomaki (1993) for European trees (i.e., Norway spruce).

Tree stability models calculate the force of the wind on a tree with knowledge of its species, height, trunk diameter at 1.4 m above the ground [i.e., diameter at breast height (DBH)], and either observed or inferred crown width and depth. The force of the wind on a segment of the tree is a function of the cross-sectional area of the tree segment, wind velocity, air density, and drag coefficient. This force causes a mechanical deflection of the crown from the vertical that, along with the weight of the deflected crown, causes a bending moment at the base of the tree. Tree stability models compare this bending moment with estimates of the critical bending moment (i.e., the force necessary to cause failure) for trunk breakage or uprooting. An individual tree's DBH and known species-dependent values for wood strength provide estimates for the critical bending moment for trunk breakage, while empirical winching studies (e.g., Peltola 2006) allow estimates of the critical bending moment for uprooting. If the bending moment exceeds either critical bending moment, the tree falls.

Holland et al. (2006) modify Peltola and Kellomaki's (1993) tree stability model with parameters for loblolly pine in the southeastern United States and produce hypothetical forest damage patterns from a simulated tornado, though the authors did not have the opportunity to compare the predicted damage patterns with empirical observations. Bech et al. (2009) examine actual tree damage patterns and compare them to classes of Letzmann's (1925) predictions, but do not include a tree stability component, thereby implicitly assuming a homogeneous stand of trees. Beck and Dotzek (2010) more fully develop this approach by examining actual tree damage patterns after two European tornadoes, using simulated vortices and the Peltola and Kellomaki (1993) tree stability model. Using this approach, the authors infer wind field parameters for the two tornadoes, demonstrating, for example, the temporal evolution of intensity along the tornado track. Karstens et al. (2013) used the Beck and Dotzek (2010) approach to produce similar estimates of tornado intensity based on analyses of treefall patterns in two tornadoes, but used the thresholds for damage to the vegetation DIs in the EF scale to create a distribution of critical wind speeds

FIG. 1. A sample of a vertical aerial photograph showing individual tree trunks, crowns, and root balls. Similar imagery covers the entire 56-mi length of both tornado tracks.

necessary to blow down trees. The present authors also attempted to use the Beck and Dotzek (2010) approach, combined with a tree stability model (Peltola and Kellomaki 1993), to characterize the near-surface wind field through rugged terrain for the same two subject tornadoes under scrutiny in this study. While this method shows great promise in relatively flat areas, unpublished research efforts indicate that the approach will not work in regions with complex topography because of the dramatic influence of the terrain on the near-surface wind field.

The present work therefore describes a novel method to infer EF-scale levels from forest damage using the degree of tree damage to a sample of trees and a coupled wind and tree resistance model. This new approach remains independent of the source of the wind. Its wind speed estimates therefore apply to any type of wind damage.

2. Data

a. Aerial imagery

Sixty-four days after the tornado outbreak, a chartered flight captured vertical aerial photographs along the entire length of both tornado tracks. The plane made two passes along each track, giving a total composite image width of about 1500 m (5000 ft) with a nominal pixel resolution of 20 cm (8 in.). These high-resolution, georeferenced images show individual tree trunks, crowns, and root balls (Fig. 1). With a few mouse clicks per tree within GIS software, each of the 130 000 clearly identifiable downed trees shown in the imagery received an electronic label marking its geographic coordinates and fall direction. Nearby standing trees also received tags recording their geographic coordinates. Together, over 448 000 fallen and standing trees received electronic labels. In addition to its use here, this unique dataset will likely provide a valuable source of observations for future studies of forest damage in complex terrain.

b. Ground surveys

Ground surveys provide valuable information that is unobtainable from the air. The authors recorded details on each tree within dozens of 400-m^2, randomly selected sample plots in each tornado track, including the tree species, trunk diameter (i.e., DBH), fall direction, snap heights, whether or not the tree remains alive, and the damage type. Damage types include ''branches broken,'' ''crown broken,'' ''snapped,'' ''bent,'' ''leaning,'' ''uprooted,'' and ''intact.'' Through 2012, the surveys collected information on 1551 individual trees in 69 plots in the CNF tornado track and 503 individual trees in 22 plots in the GSMNP track. Tree heights for a small selection of trees in the CNF tornado track were measured in a variety of ways, depending on tree size and position. One method utilizes a telescoping fiberglass pole that can measure the heights of relatively short trees. Another option involves a simple tape measure to determine the heights of uprooted trees on the ground. For trees that have snapped, the total height is the sum of the height of the stump and the length of the remaining nearby trunk and crown. Other options include an optical rangefinder and simple geometry. The following analysis assumes that the samples obtained in the ground surveys represent the species composition and size distribution of the trees in each respective forest.

3. Methodology

For each tornado track, a statistical resampling procedure begins by randomly drawing, with replacement, a small sample of 100 trees from the database of trees observed during the ground surveys in that particular forest. Then, a coupled wind and tree resistance model (Peltola and Kellomaki 1993) determines the percentage of trees that fall in this fictitious plot for a set of wind speeds ranging from light breezes to extreme wind speeds. The model works by first calculating the lateral displacement of each tree under the influence of a particular wind-induced force, and then the resulting turning moment (or torque) at the base of the stem. If the turning moment exceeds the tree's trunk or root system resistance to breakage or overturning, the tree falls. Kretschmann (2010) and Panshin and de Zeeuw (1970) provide the modulus of rupture and the modulus of elasticity for each species. Since values for the modulus of rupture typically represent laboratory-tested values

for clean, knot-free wood, trunk resistance here is reduced to 85% of the ideal trunk strength, following the recommendations of Gardiner et al. (2000).

Application of the Peltola and Kellomaki (1993) tree stability model requires knowledge of the species, height, DBH, crown depth, and crown radius for each tree. Since the ground surveys could not possibly measure all of these parameters, it becomes necessary to augment the measurements with estimates of tree height and crown shape for each tree. Observed tree heights are available for 788 (i.e., approximately half) of the trees surveyed in the CNF track. For all other surveyed trees, an estimate of tree height is derived from a species-dependent height–DBH allometry (Purves et al. 2007). Comparisons between observed and estimated tree heights (not shown) indicate that the height estimates are reasonable. The ideal tree distribution (ITD) model (Purves et al. 2007) determines the crown shapes within a stand of trees by selecting the height of the canopy above the ground at which the total of the exposed crown areas is equal to the ground area. The calculation accounts for the species dependence of the crown radius and crown depth for each tree. As implemented here, the ground area matches the 400-m^2 area of the ground survey plots, and the ITD model calculates crown shapes for the observed trees in each plot. Therefore, each ground survey plot receives an estimate of the tree heights and crown shapes for the actual trees in that plot. Trees with a total height that is less than the calculated height of the canopy bottom receive a fixed species-dependent crown radius. In the original ITD model, these understory trees also receive a fixed crown depth. Empirical evidence based on numerous ground surveys suggests that, regardless of species, observed tree crowns constitute approximately the upper 50% of the total tree height for canopy trees, with understory crown depths of around 30%. Understory trees here, therefore, receive a more reasonable estimate for crown depth of 30% of their total height. Taken together, the species, height, DBH, crown radius, and crown depth allow the tree stability model to calculate the wind load on each tree. After comparing the wind load with the resistance of the trunk or root system, the tree stability model ultimately determines whether or not the tree falls at a given wind speed.

Each wind speed value, separated by 1 $m\,s^{-1}$ increments, corresponds with a particular percentage of fallen trees within each random sample of 100 trees drawn from the database of observed trees. Repeating the resampling procedure 10 000 times yields a symmetric sampling distribution that closely approximates a Gaussian probability density function and that describes treefall percentages for each wind speed (Fig. 2). The shaded region in Fig. 2a, for example, corresponds with a wind speed of 50 $m\,s^{-1}$ in the GSMNP forest. This wind speed knocked down an average of 57.1% of the trees in each of the 10 000 random sample plots, with damage ranging from a minimum of 38 to a maximum of 74 of the 100 trees knocked down, and with a standard deviation of 4.98 trees.

In small sections of the real forest, the assignment of an EF-scale level proceeds by assessing the observed percentage of fallen trees. These subplots measure 100 m $\times$ 100 m, a scale chosen both to approximate roughly the number of trees in the fictitious plots and to provide adequate spatial coverage while still capturing spatial variations in damage severity. The most probable wind speed that produced the damage in each subplot then corresponds with the associated sampling distribution, with its peak matching the observed percentage of trees blown down in that forest section (Fig. 3). To avoid undersampling, the assignment procedure ignores subplots with 10 or fewer total trees. Excluding such subplots, each subplot on average contains 70 total trees, with averages of 85 trees and 59 trees per subplot in the GSMNP and CNF tracks, respectively.

4. Maps of EF-scale damage

Application of this estimation procedure to the entire length of both tornado tracks yields maps showing estimates of the EF-scale ratings based on forest damage severity (Fig. 4). The procedure also captures the variability in the intensity of each tornado along its track and appropriately assigns lower EF-scale levels on the outside edges of the damage tracks and assigns higher EF-scale levels nearer to the center of each track. Notably, both tornadoes produced damage rated EF5 by the estimation technique, where nearly 100% of the trees were blown down in the small subplots. Also, a few subplots rated EF5 border subplots with ratings of EF0 or no rating at all. This result is consistent with the authors' own observations and with those of Blanchard (2013), who also studied forest damage from tornadoes and noted sharp spatial gradients in the level of damage within the forest. The small-scale variability also stems from the relationship between the surface flow field and the complex terrain.

Figure 5 shows a section of the GSMNP tornado track near the intersection of the Hatcher Mountain Trail and the Little Bottoms Trail along Abrams Creek (see the inset in Fig. 4). The EF-scale ratings appear overlaid on the aerial imagery, showing the standing and fallen trees. In this section of the forest, the tornado moved from the bottom left to the top right (i.e., northeast), first descending a mountain toward Abrams Creek, then

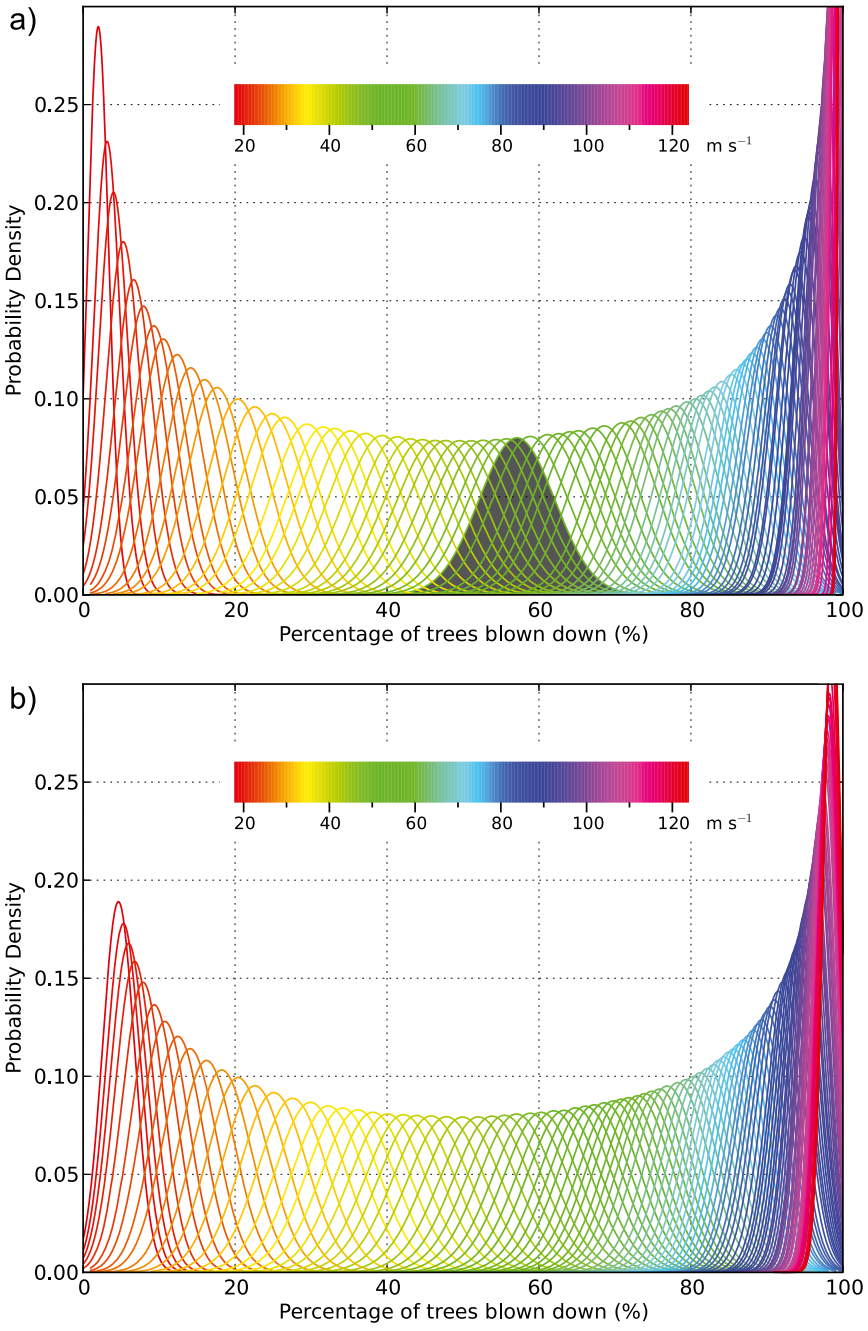

FIG. 2. Probability density functions describing the percentage of trees blown down at various wind speeds in 10 000 fictitious sample plots using trees drawn from a database of observed trees in the (a) GSMNP and (b) CNF. The shaded region in (a) corresponds with the example in the text.

ascending Hatcher Mountain toward the top right of the image. As the tornado crossed Abrams Creek and ran into the steep hillside, the flow likely constricted and accelerated. The tornado completely destroyed the dense forest canopy on the hillside facing the oncoming tornado (Fig. 6), and the wind accelerated up a small valley to the north of the hill, but left the trees on the back side of the hill nearly untouched. The automated EF-scale estimation procedure captures the variability in the damage on this small scale.

The technique also captures the likely wind speeds responsible for the damage, as shown in Fig. 6. Here, the bottom-left portion of the image corresponds with a subplot to which the estimation procedure assigned

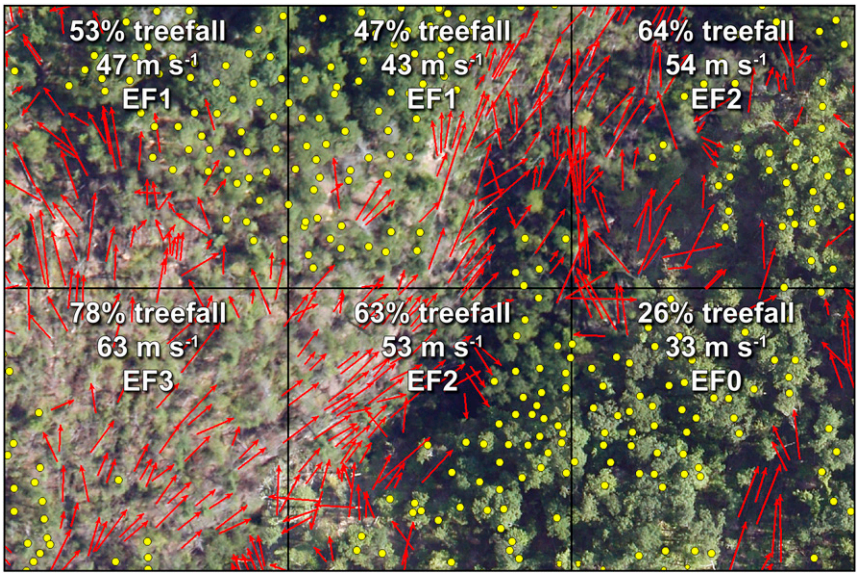

FIG. 3. A section of the GSMNP tornado track illustrating the assignment procedure for EF-scale levels. Red arrows represent fallen trees, yellow dots represent standing trees, and the black lines show the boundaries of the 100 m × 100 m subplots. At the top left, for example, the tornado knocked down 53% of the trees in the subplot, corresponding with a most probable wind speed of 47 m s^{-1} and an EF-scale rating of EF1.

a wind speed of 64 m s^{-1} (143 mi h^{-1}), equivalent to a rating of EF3, and the right two-thirds of the image corresponds with a subplot with an estimated wind speed of 87 m s^{-1} (195 mi h^{-1}) and a rating of EF4. This result remains entirely consistent with the levels of damage observed in person in this area of the forest. The highest degree of damage associated with the vegetation DIs of the EF scale describes debarked trees with only the stubs of the largest branches remaining. For hardwood trees, the expected wind speed associated with this degree of damage is 64 m s^{-1} (143 mi h^{-1}), and for softwood trees the expected wind speed is 59 m s^{-1} (131 mi h^{-1}). The authors observed numerous examples of stubbed trees along this section of the tornado track, yet no obvious examples of debarking. However, debarking may primarily occur only in urban and residential areas as a result of the increased availability of damaging debris compared with a forested environment (Peterson and Godfrey 2014).

5. Discussion

The technique described here uses tree damage severity following tornadoes or other windstorms to estimate the wind speed responsible for the damage. The results of the automated analysis remain consistent with the authors' ground observations in both tornado tracks and capture the spatial variability of the damage. Notably, the analysis requires a balanced spatial distribution of tagged trees in each subplot (i.e., approximately every *n*th tree must be tagged) in order to avoid corrupting the calculation of the percentage of the fallen trees within that subplot. However, application of a filtering algorithm that considers only a certain number of trees within a given area could easily solve the problem by accounting for spatial density variations resulting from two different tree labelers or analyses viewed at different zoom levels or pixel resolutions. The wind speed assignment procedure also assumes a uniform wind speed across each subplot, similar to the assumptions of Canham et al. (2001). This bold assumption ignores the fact that the terrain influences the near-surface tornadic flow field on small spatial scales, as is clearly evident in Fig. 3. The assigned wind speed therefore represents a smoothed value for the wind speed in each subplot. The chosen areal coverage of the subplots thus necessitates a balance between the requirement for a sufficiently large sample of trees and the requirement for sufficiently small spatial coverage to avoid excessive smoothing.

The individual probability density functions that describe treefall percentages for each wind speed value depend upon the results of the tree stability model. This model in turn depends strongly on the published modulus of rupture and the modulus of elasticity for each tree species, mostly determined through laboratory studies on homogeneous, straight-grained wood. Real trees may have a different response than that given by the model when subjected to strong winds. Empirical winching studies can help to determine the mechanical

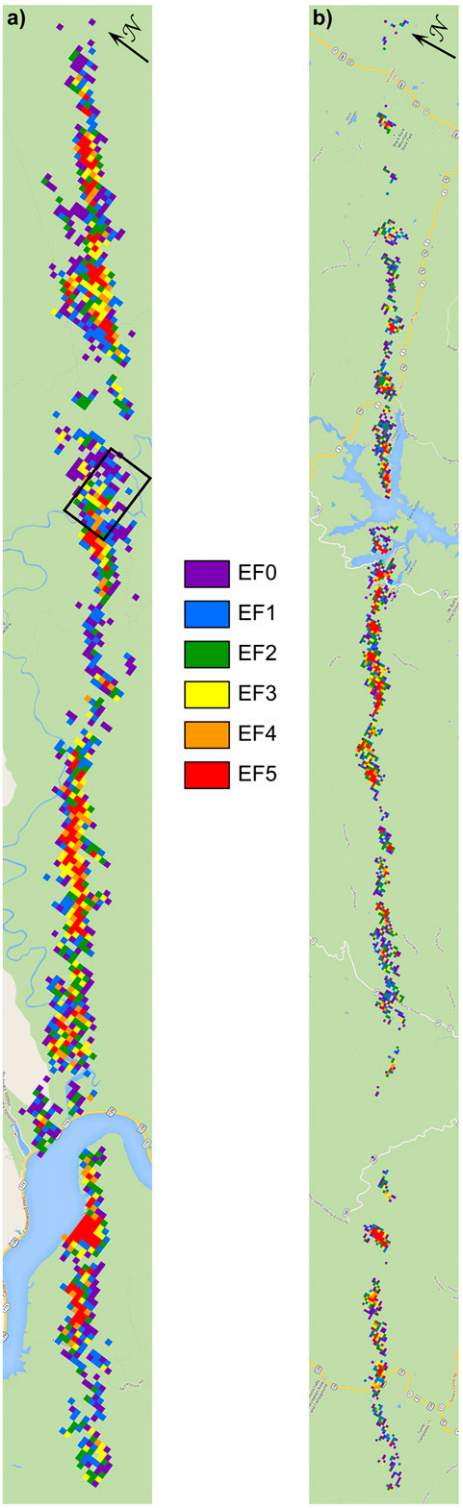

FIG. 4. EF-scale ratings assigned to small subplots along the length of the (a) GSMNP and (b) CNF tornado tracks. The inset in (a) is the region shown in Fig. 5. Note that the scales differ in each map. The GSMNP track is 18 mi long and the CNF track is 38 mi long.

properties of real trees by pulling on the trunks with a known force until they break or uproot (Peterson and Claassen 2013; Cannon et al. 2015). While this technique remains very rare in the United States, researchers in Canada, the United Kingdom, and Scandinavia practice the technique more commonly. Further winching studies on trees found in U.S. forests will improve our quantitative understanding of the dependence of both tree size and species on the wind resistance of these trees. With such improved estimates of tree strength, the tree stability model could more reliably determine the fate of a particular tree at a given wind speed, thereby altering the empirical sampling distributions employed in the approach presented here.

Additionally, this estimation technique easily allows for the calculation of confidence intervals on each wind speed estimate. First, each of the fictitious sample plots receives a wind speed assignment for the complete range of possible percentages of downed trees from 0% to 100%. For example, if the model knocks down 52% of the trees for a wind speed of 46 m s^{-1} and 54% of the trees for the next higher wind speed of 47 m s^{-1} in a particular sample, then the higher wind speed of 47 m s^{-1} must also knock down 53% of the trees. With this 10 000-member sampling distribution for each percentage of trees blown down, the 95% confidence interval is the range defined by the 250th and the 9750th sorted samples. For example, the most probable wind speed for an observed treefall percentage of 76% in a subplot in the GSMNP track is 62 m s^{-1} with a 95% confidence interval defined by the range 56–70 m s^{-1}. This method can therefore provide a range of possible wind speeds, and corresponding EF-scale levels, responsible for a given degree of damage observed in a forest with a particular species composition and size distribution, as shown in Fig. 7 for the GSMNP forest. The wind speed estimates and confidence intervals will vary from those shown in Fig. 7 for different tree populations.

This objective wind estimation technique differs from the traditional EF-scale approach by removing subjectivity. Wind speed estimates depend only on the percentage of downed trees within a small area and other measurable factors. Additionally, the vegetation DIs of the EF scale suffer from the limitation that EF3 is the highest possible rating, as well as a number of other concerns outlined by Peterson and Godfrey (2014). In contrast, the approach outlined here allows ratings up to EF5 within forests. However, one would expect that the number of subplots assigned an EF0 rating would exceed the number assigned EF1, and that each stronger rating would be assigned to fewer subplots. This is true in each tornado track up to a rating of EF4, but the number of EF5 ratings assigned to individual subplots using this approach actually exceeds the number of EF4

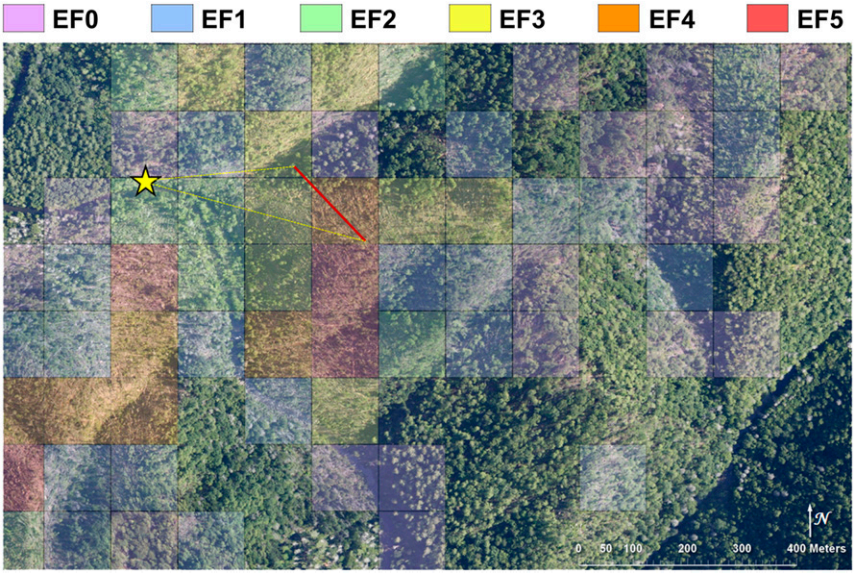

FIG. 5. EF-scale estimates near the intersection of the Hatcher Mountain Trail and the Little Bottoms Trail along Abrams Creek in the GSMNP (see inset in Fig. 4). The star indicates the location of the photographer and the red line corresponds with the field of view in the photo shown in Fig. 6.

ratings, suggesting that the scheme may overestimate the wind speeds necessary to blow down trees. Values in the tree stability model, particularly for the critical bending moment for trunk breakage or uprooting, may therefore need some revision to reduce the estimated wind speed associated with extreme levels of damage.

A spatial shift in the location of each subplot does not appear to make a substantial impact on either the overall distribution of EF-scale levels along the tornado track or the general character of the visual presentation of the damage map. The area of the subplot, however, must be chosen carefully. The distributions of EF-scale levels remain similar whether the subplot dimension is 75 m × 75 m or 200 m × 200 m, so the area of each grid cell does not appear to impact the overall results significantly. The trade-off, however, is decreased resolution with larger grid sizes and the inability to capture spatial variations in damage severity. A visual assessment of damage photos overlaid with EF-scale estimates shows that maps with a doubled grid dimension to 200 m × 200 m (i.e., a quadrupled area) clearly suffer from this lack of spatial detail. On the other hand, a smaller grid dimension of 75 m × 75 m does not provide adequate spatial coverage for each subplot and can dramatically inflate the number of subplots with EF5 ratings. For the density of trees in the GMSNP and CNF forests, subplots measuring between 100 m × 100 m and 150 m × 150 m contain a rough average of approximately 100 trees and produce the most reasonable results.

This approach does not account for the duration of maximum wind speeds. While there is some evidence to suggest that a species-dependent difference in resistance to long-duration wind speeds, such as in hurricanes, compared with short-duration gusts may be due to particular leaf shape or trunk properties (e.g., Xi et al. 2008), the relationship between the duration of the wind and the damage to trees remains unknown. Therefore, a modification of this method to account for wind duration would have no quantitative basis given current knowledge, though future research could inform suitable refinements.

Soil and rooting conditions may also influence a tree's resistance to strong winds. In the long term, soil drainage and soil depth both influence tree stability because they

FIG. 6. Photograph, taken 27 months after the GSMNP tornado, looking east showing a steep slope that the damage estimation technique labeled EF3 (left third) and EF4 (right two-thirds). The tornado completely destroyed the dense forest canopy.

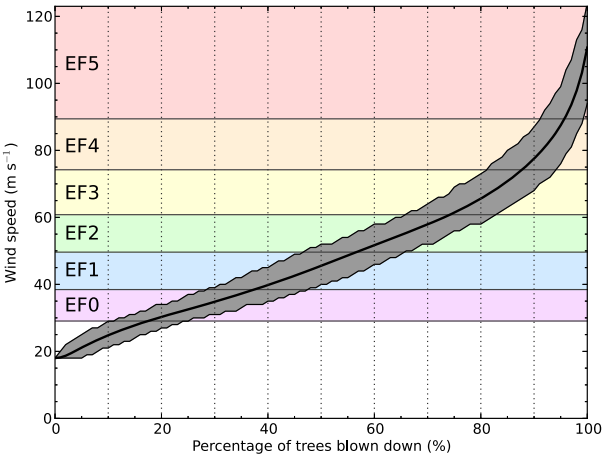

FIG. 7. Wind speed estimates (thick line) for the GSMNP forest as a function of the percentage of trees blown down in each fictitious sample plot. The gray-shaded region denotes the 95% confidence interval for each percentage of trees blown down, and the colored regions represent the wind speeds associated with each EF-scale level.

can limit rooting depth (Nicoll et al. 2006). Soil moisture conditions that vary according to precipitation, drainage conditions, and soil texture can strongly influence resistance to uprooting, which decreases nonlinearly with increasing soil water content (Kamimura et al. 2012). However, given the very fine spatial scale of these variables, the authors chose not to sample the soils as part of the ground surveys. Personal observations during these surveys suggest that very little of the tornado tracks include permanent wetlands, so the results presented here are likely not unduly influenced by long-term soil saturation. Nevertheless, application of this or similar approaches would need to account for the fact that trees will fall more easily in saturated soils, so downward adjustments to the estimated wind speeds would be appropriate in such circumstances.

Given the intense manual labor involved with both the ground surveys and the labeling process for each tree via GIS software, this study primarily serves only as a proof of concept to demonstrate the feasibility of such an EF-scale estimation technique. However, this approach may easily lead to methods for the straightforward estimation of EF-scale levels in remote or inaccessible locations. To provide useful EF-scale estimates in a short time frame, the method requires the speedy acquisition of high-resolution vertical aerial photographs or satellite imagery. Ideally, an automated tree-tagging algorithm could quickly process the georeferenced imagery and determine the locations of both standing and fallen trees. Alternatively, a supervised classification algorithm, as in Cannon et al. (2016), could quickly determine damage severity based on aerial or satellite imagery, followed by application of the technique described here to assign EF-scale levels. A user may also choose to target only specific regions within the aerial imagery that exhibit the most extensive tree damage in order to obtain a maximum EF-scale rating. Additionally, predetermined wind speed estimates that correspond with various degrees of forest damage would require representative samples of the tree species and size composition obtained from prestorm ground surveys in various forested regions, but would enable rapid application of this approach to wind estimation.

Acknowledgments. The authors wish to thank Michael Goldsbury and Dawn Pomeroy for tagging nearly half a million trees in their spare time and the National Park Service and U.S. Forest Service for granting access to remote regions of the Great Smoky Mountains National Park and the Chattahoochee National Forest. This work benefited from data acquired during a project funded by NSF RAPID Grant AGS-1141926 and from additional support by NOAA Grant NA15OAR4590227.

REFERENCES

Bech, J., M. Gayà, M. Aran, F. Figuerola, J. Amaro, and J. Arús, 2009: Tornado damage analysis of a forest area using site survey observations, radar data and a simple analytical vortex model. *Atmos. Res.*, **93**, 118–130, doi:10.1016/j.atmosres.2008.10.016.

Beck, V., and N. Dotzek, 2010: Reconstruction of near-surface tornado wind fields from forest damage. *J. Appl. Meteor. Climatol.*, **49**, 1517–1537, doi:10.1175/2010JAMC2254.1.

Blanchard, D. O., 2013: A comparison of wind speed and forest damage associated with tornadoes in northern Arizona. *Wea. Forecasting*, **28**, 408–417, doi:10.1175/WAF-D-12-00046.1.

Bluestein, H. B., 2000: A tornadic supercell over elevated, complex terrain: The Divide, Colorado, storm of 12 July 1996. *Mon. Wea. Rev.*, **128**, 795–809, doi:10.1175/1520-0493(2000)128<0795:ATSOEC>2.0.CO;2.

Bosart, L. F., A. Seimon, K. D. LaPenta, and M. J. Dickinson, 2006: Supercell tornadogenesis over complex terrain: The Great Barrington, Massachusetts, tornado on 29 May 1995. *Wea. Forecasting*, **21**, 897–922, doi:10.1175/WAF957.1.

Canham, C. D., M. J. Papaik, and E. F. Latty, 2001: Interspecific variation in susceptibility to windthrow as a function of tree size and storm severity for northern temperate tree species. *Can. J. For. Res.*, **31**, 1–10, doi:10.1139/x00-124.

Cannon, J. B., M. E. Barrett, and C. J. Peterson, 2015: The effect of species, size, failure mode, and fire-scarring on tree stability. *For. Ecol. Manage.*, **356**, 196–203, doi:10.1016/j.foreco.2015.07.014.

——, J. Hepinstall-Cymerman, C. M. Godfrey, and C. J. Peterson, 2016: Landscape-scale patterns of forest tornado damage in mountainous terrain. *Landscape Ecol.*, **31**, 2097–2114, doi:10.1007/s10980-016-0384-8.

Dessens, J., 1972: Influence of ground roughness on tornadoes: A laboratory simulation. *J. Appl. Meteor.*, **11**, 72–75, doi:10.1175/1520-0450(1972)011<0072:IOGROT>2.0.CO;2.

Dunn, L. B., and S. V. Vasiloff, 2001: Tornadogenesis and operational considerations of the 11 August 1999 Salt Lake City tornado as seen from two different Doppler radars. *Wea. Forecasting*, **16**, 377–398, doi:10.1175/1520-0434(2001)016<0377:TAOCOT>2.0.CO;2.

Edwards, R., J. G. LaDue, J. T. Ferree, K. Scharfenberg, C. Maier, and W. L. Coulbourne, 2013: Tornado intensity estimation: Past, present, and future. *Bull. Amer. Meteor. Soc.*, **94**, 641–653, doi:10.1175/BAMS-D-11-00006.1.

Fiedler, B. H., 1994: The thermodynamic speed limit and its violation in axisymmetric numerical simulations of tornado-like vortices. *Atmos.–Ocean*, **32**, 335–359, doi:10.1080/07055900.1994.9649501.

——, and R. Rotunno, 1986: A theory for the maximum windspeeds in tornado-like vortices. *J. Atmos. Sci.*, **43**, 2328–2340, doi:10.1175/1520-0469(1986)043<2328:ATOTMW>2.0.CO;2.

Forbes, G. S., 1998: Topographic influences on tornadoes in Pennsylvania. Preprints, *19th Conf. on Severe Local Storms*, Minneapolis, MN, Amer. Meteor. Soc., 269–272.

Fujita, T. T., 1989: The Teton–Yellowstone tornado of 21 July 1987. *Mon. Wea. Rev.*, **117**, 1913–1940, doi:10.1175/1520-0493(1989)117<1913:TTYTOJ>2.0.CO;2.

Gardiner, B., H. Peltola, and S. Kellomaki, 2000: Comparison of two models for predicting the critical wind speeds required to damage coniferous trees. *Ecol. Modell.*, **129**, 1–23, doi:10.1016/S0304-3800(00)00220-9.

Holland, A. P., A. J. Riordan, and E. C. Franklin, 2006: A simple model for simulating tornado damage in forests. *J. Appl. Meteor. Climatol.*, **45**, 1597–1611, doi:10.1175/JAM2413.1.

Homar, V., M. Gayà, R. Romero, C. Ramis, and S. Alonso, 2003: Tornadoes over complex terrain: An analysis of the 28th August 1999 tornadic event in eastern Spain. *Atmos. Res.*, **67–68**, 301–317, doi:10.1016/S0169-8095(03)00064-4.

Kamimura, K., K. Kitagawa, S. Saito, and H. Mizunaga, 2012: Root anchorage of hinoki (*Chamaecyparis obtuse* (Sieb. Et Zucc.) Endl.) under the combined loading of wind and rapidly supplied water on soil: Analyses based on tree-pulling experiments. *Eur. J. For. Res.*, **131**, 219–227, doi:10.1007/s10342-011-0508-2.

Karstens, C. D., W. A. Gallus Jr., B. D. Lee, and C. A. Finley, 2013: Analysis of tornado-induced tree fall using aerial photography from the Joplin, Missouri, and Tuscaloosa–Birmingham, Alabama, tornadoes of 2011. *J. Appl. Meteor. Climatol.*, **52**, 1049–1068, doi:10.1175/JAMC-D-12-0206.1.

Kretschmann, D. E., 2010: Mechanical properties of wood. *Wood Handbook: Wood as an Engineering Material*, R. J. Ross, Ed., Forest Products Laboratory General Tech. Rep. FPL-GTR-190, Forest Service, 5-1–5-46. [Available online at http://www.fpl.fs.fed.us/documnts/fplgtr/fplgtr190/chapter_05.pdf.]

LaPenta, K. D., L. F. Bosart, T. J. Galarneau, and M. J. Dickinson, 2005: A multiscale examination of the 31 May 1998 Mechanicville, New York, F3 tornado. *Wea. Forecasting*, **20**, 494–516, doi:10.1175/WAF875.1.

Letzmann, J. P., 1925: Fortschreitende Luftwirbel (Advancing air vortices). *Meteor. Z.*, **42**, 41–52.

Lewellen, D. C., 2012: Effects of topography on tornado dynamics: A simulation study. *26th Conf. on Severe Local Storms*, Nashville, TN, Amer. Meteor. Soc., 4B.1. [Available online at https://ams.confex.com/ams/26SLS/webprogram/Paper211460.html.]

——, and W. S. Lewellen, 2007: Near-surface intensification of tornado vortices. *J. Atmos. Sci.*, **64**, 2176–2194, doi:10.1175/JAS3965.1.

——, ——, and J. Xia, 2000: The influence of a local swirl ratio on tornado intensification near the surface. *J. Atmos. Sci.*, **57**, 527–544, doi:10.1175/1520-0469(2000)057<0527:TIOALS>2.0.CO;2.

——, B. Gong, and W. S. Lewellen, 2008: Effects of finescale debris on near-surface tornado dynamics. *J. Atmos. Sci.*, **65**, 3247–3262, doi:10.1175/2008JAS2686.1.

Lewellen, W. S., D. C. Lewellen, and R. I. Sykes, 1997: Large-eddy simulation of a tornado's interaction with the surface. *J. Atmos. Sci.*, **54**, 581–605, doi:10.1175/1520-0469(1997)054<0581:LESOAT>2.0.CO;2.

Markowski, P. M., and N. Dotzek, 2011: A numerical study of the effects of orography on supercells. *Atmos. Res.*, **100**, 457–478, doi:10.1016/j.atmosres.2010.12.027.

Nicoll, B. C., B. A. Gardiner, B. Rayner, and A. J. Peace, 2006: Anchorage of coniferous trees in relation to species, soil type, and rooting depth. *Can. J. For. Res.*, **36**, 1871–1883, doi:10.1139/x06-072.

Oswalt, S. N., W. B. Smith, P. D. Miles, and S. A. Pugh, 2014: Forest resources of the United States, 2012: A technical document supporting the Forest Service update of the 2010 RPA assessment. U.S. Forest Service General Tech. Rep. WO-91, 218 pp. [Available online at http://www.fs.fed.us/sites/default/files/legacy_files/media/types/publication/field_pdf/GTR-WO-91.pdf.]

Panshin, A. J., and C. de Zeeuw, 1970: *Textbook of Wood Technology*. 3rd ed. McGraw-Hill, 705 pp.

Peltola, H., 2006: Mechanical stability of trees under static loads. *Amer. J. Bot.*, **93**, 1501–1511, doi:10.3732/ajb.93.10.1501.

——, and S. Kellomaki, 1993: A mechanistic model for calculating windthrow and stem breakage of Scots pine at stand edge. *Silva Fenn.*, **27**, 99–111, doi:10.14214/sf.a15665.

Peterson, C. J., and V. Claassen, 2013: An evaluation of the stability of Quercus lobata and Populus fremontii on river levees assessed using static winching tests. *Forestry*, **86**, 201–209, doi:10.1093/forestry/cps080.

——, and C. M. Godfrey, 2014: Side-by-side tree and house damage in the May 2013 Moore, OK EF5 tornado: Lessons for the enhanced Fujita scale. *Special Symp. on Severe Local Storms: The Current State of the Science and Understanding Impacts*, Atlanta, GA, Amer. Meteor. Soc., 831. [Available online at https://ams.confex.com/ams/94Annual/webprogram/Paper241535.html.]

Purves, D. W., J. W. Lichstein, and S. W. Pacala, 2007: Crown plasticity and competition for canopy space: A new spatially implicit model parameterized for 250 North American tree species. *PLoS One*, **2**, e870, doi:10.1371/journal.pone.0000870.

Roberts, B., M. Xue, A. D. Schenkman, and D. T. Dawson II, 2016: The role of surface drag in tornadogenesis within an idealized supercell simulation. *J. Atmos. Sci.*, **73**, 3371–3395, doi:10.1175/JAS-D-15-0332.1.

Schenkman, A. D., M. Xue, and M. Hu, 2014: Tornadogenesis in a high-resolution simulation of the 8 May 2003 Oklahoma City supercell. *J. Atmos. Sci.*, **71**, 130–154, doi:10.1175/JAS-D-13-073.1.

Smith, G. M., Y.-L. Lin, and Y. Rastigejev, 2016: Orographic effects on supercell: Development and structure, intensity and tracking. *Environ. Nat. Resour. Res.*, **6**, 76–91.

WSEC, 2006: A recommendation for an enhanced Fujita scale (EF-scale), revision 2. Wind Science and Engineering Center Rep., Texas Tech University, Lubbock, TX, 95 pp. [Available online at http://www.depts.ttu.edu/nwi/pubs/fscale/efscale.pdf.]

Xi, W., R. K. Peet, J. K. DeCoster, and D. L. Urban, 2008: Tree damage risk factors associated with large, infrequent wind disturbances of Carolina forests. *Forestry*, **81**, 317–334, doi:10.1093/forestry/cpn020.